



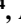











Combining Top-Down and Bottom-Up Approaches to Evaluate Recent Trends and Seasonal Patterns in UK N₂O Emissions

Key Points:

- Atmospheric N₂O measurements from 2013 to 2022 are used to evaluate the UK's reported emissions using two inverse methods
- Emissions derived from atmospheric data are on average 22%–51% higher than the UK's national emissions inventory values across 2013–2022
- Agreement between the average top-down and bottom-up seasonal emissions was improved by decreasing bottom-up synthetic fertilizer emissions

Eric Saboya¹ , **Alistair J. Manning**² , **Peter Levy**³ , **Kieran M. Stanley**⁴ , **Joseph Pitt**⁴, **Dickon Young**⁴ , **Daniel Say**⁴, **Aoife Grant**⁴, **Tim Arnold**^{5,6,7} , **Chris Rennick**⁵ , **Samuel J. Tomlinson**⁸ , **Edward J. Carnell**³, **Yuri Artoli**⁹ , **Ann Stavart**¹⁰ , **T. Gerard Spain**¹¹, **Simon O'Doherty**⁴, **Matthew Rigby**⁴ , and **Anita L. Ganesan**¹ 

¹School of Geographical Sciences, University of Bristol, Bristol, UK, ²Met Office Hadley Centre, Exeter, UK, ³UK Centre for Ecology and Hydrology, Edinburgh, UK, ⁴School of Chemistry, University of Bristol, Bristol, UK, ⁵National Physical Laboratory, Teddington, UK, ⁶School of GeoSciences, University of Edinburgh, Edinburgh, UK, ⁷Department of Physical Geography and Ecosystem Science, Lund University, Lund, Sweden, ⁸UK Centre for Ecology and Hydrology, Lancaster, UK, ⁹Plymouth Marine Laboratory, Plymouth, UK, ¹⁰Climate Science Centre, CSIRO Oceans and Atmosphere, Aspendale, VIC, Australia, ¹¹School of Natural Sciences, University of Galway, Galway, Ireland

Supporting Information:

Supporting Information may be found in the online version of this article.

Correspondence to:

E. Saboya and A. L. Ganesan,
eric.saboya@bristol.ac.uk;
anita.ganesan@bristol.ac.uk

Citation:

Saboya, E., Manning, A. J., Levy, P., Stanley, K. M., Pitt, J., Young, D., et al. (2024). Combining top-down and bottom-up approaches to evaluate recent trends and seasonal patterns in UK N₂O emissions. *Journal of Geophysical Research: Atmospheres*, 129, e2024JD040785. <https://doi.org/10.1029/2024JD040785>

Received 11 JAN 2024

Accepted 26 JUN 2024

Author Contributions:

Conceptualization: Eric Saboya, Alistair J. Manning, Peter Levy, Matthew Rigby, Anita L. Ganesan

Data curation: Peter Levy, Kieran M. Stanley, Joseph Pitt, Dickon Young, Aoife Grant, Tim Arnold, Chris Rennick, Ann Stavart, T. Gerard Spain, Simon O'Doherty

Formal analysis: Eric Saboya

Abstract Atmospheric trace gas measurements can be used to independently assess national greenhouse gas inventories through inverse modeling. Atmospheric nitrous oxide (N₂O) measurements made in the United Kingdom (UK) and Republic of Ireland are used to derive monthly N₂O emissions for 2013–2022 using two different inverse methods. We find mean UK emissions of 90.5 ± 23.0 (1σ) and 111.7 ± 32.1 (1σ) Gg N₂O yr⁻¹ for 2013–2022, and corresponding trends of -0.68 ± 0.48 (1σ) Gg N₂O yr⁻² and -2.10 ± 0.72 (1σ) Gg N₂O yr⁻², respectively, for the two inverse methods. The UK National Atmospheric Emissions Inventory (NAEI) reported mean N₂O emissions of 73.9 ± 1.7 (1σ) Gg N₂O yr⁻¹ across this period, which is 22%–51% smaller than the emissions derived from atmospheric data. We infer a pronounced seasonal cycle in N₂O emissions, with a peak occurring in the spring and a second smaller peak in the late summer for certain years. The springtime peak has a long seasonal decline that contrasts with the sharp rise and fall of N₂O emissions estimated from the bottom-up UK Emissions Model (UKEM). Bayesian inference is used to minimize the seasonal cycle mismatch between the average top-down (atmospheric data-based) and bottom-up (process model and inventory-based) seasonal emissions at a sub-sector level. Increasing agricultural manure management and decreasing synthetic fertilizer N₂O emissions reduces some of the discrepancy between the average top-down and bottom-up seasonal cycles. Other possibilities could also explain these discrepancies, such as missing emissions from NH₃ deposition, but these require further investigation.

Plain Language Summary Atmospheric nitrous oxide (N₂O) is an important greenhouse gas and ozone depleting substance. Atmospheric N₂O measurements made in the United Kingdom (UK) and Republic of Ireland were used to derive UK N₂O emissions for 2013–2022 using two inverse methods. UK emissions derived using atmospheric N₂O measurements were on average 22%–51% higher than emissions reported in the UK National Atmospheric Emissions Inventory. A pronounced seasonal cycle in N₂O emissions is inferred from the atmospheric N₂O observations which contrasts the seasonal N₂O emissions estimated in the bottom-up (process model and inventory-based) UK Emissions Model (UKEM). We find increasing agricultural manure management N₂O emissions and decreasing synthetic fertilizer N₂O emissions reduces some of the discrepancy between the seasonal cycles.

1. Introduction

Atmospheric nitrous oxide (N₂O) is an important, long-lived greenhouse gas (GHG) that also contributes to the depletion of stratospheric ozone. Whilst global emissions of N₂O are well-constrained at around 17 Tg N₂O-N yr⁻¹ (27 Tg N₂O yr⁻¹; Stell et al., 2022; Tian et al., 2020; Thompson et al., 2019; Wells et al., 2018) there are significant regional-scale differences between top-down (atmospheric data-based) and bottom-up (process model and inventory-based) N₂O emissions estimates (e.g., Jeong et al., 2018; Thompson et al., 2014; Wells et al., 2018).

The United Kingdom's (UK's) bottom-up N₂O emissions are reported in the UK National Atmospheric Emissions Inventory (NAEI; Ricardo Energy and Environment, 2019) each year which inform the National Inventory

© 2024 Crown copyright and The Author (s). This article is published with the permission of the Controller of HMSO and the King's Printer for Scotland.

This is an open access article under the terms of the [Creative Commons Attribution License](https://creativecommons.org/licenses/by/4.0/), which permits use, distribution and reproduction in any medium, provided the original work is properly cited.

Funding acquisition: Simon O'Doherty, Matthew Rigby, Anita L. Ganesan
Investigation: Eric Saboya, Alistair J. Manning
Methodology: Eric Saboya, Alistair J. Manning, Peter Levy, Anita L. Ganesan
Project administration: Simon O'Doherty, Anita L. Ganesan
Resources: Peter Levy, Kieran M. Stanley, Joseph Pitt, Dickon Young, Daniel Say, Tim Arnold, Chris Rennick, Samuel J. Tomlinson, Edward J. Carnell, Yuri Artoli, T. Gerard Spain, Simon O'Doherty
Supervision: Alistair J. Manning, Matthew Rigby, Anita L. Ganesan
Writing – original draft: Eric Saboya
Writing – review & editing: Eric Saboya, Alistair J. Manning, Peter Levy, Kieran M. Stanley, Joseph Pitt, Dickon Young, Aoife Grant, Tim Arnold, Chris Rennick, Ann Stavart, Simon O'Doherty, Matthew Rigby, Anita L. Ganesan

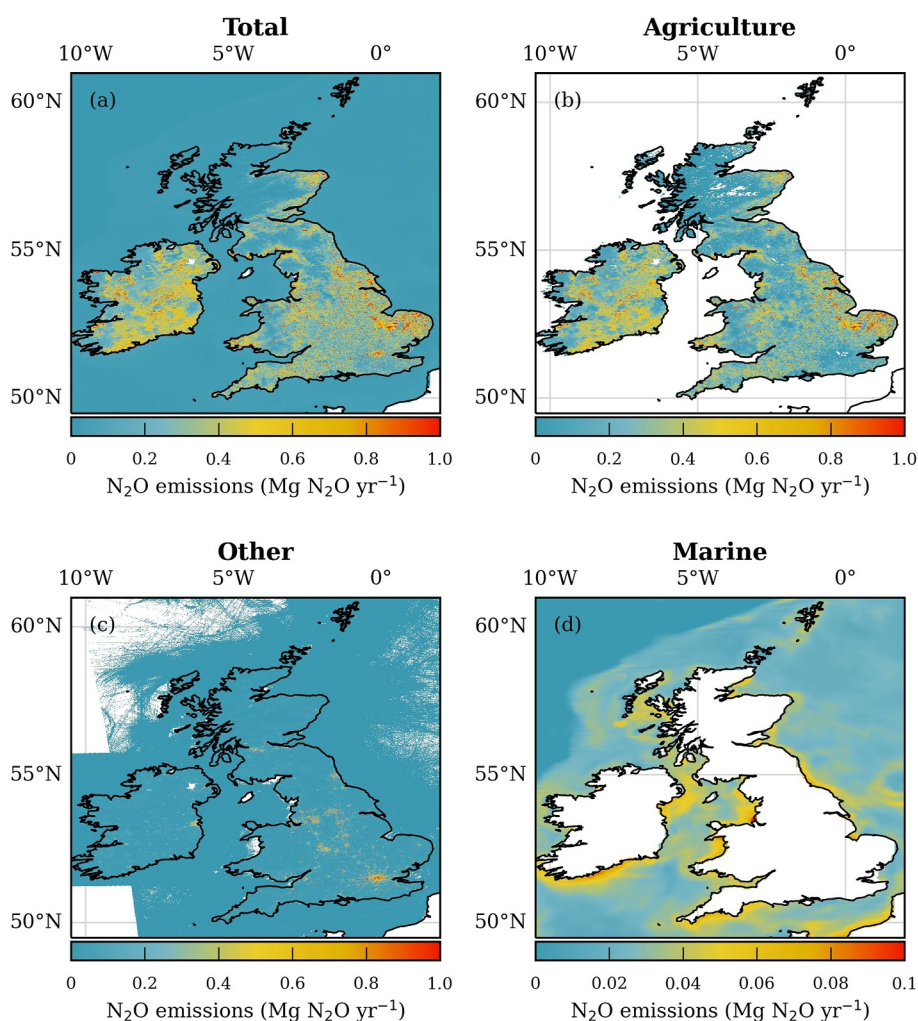


Figure 1. Bottom-up UKEM (a) total; (b) agricultural; (c) other anthropogenic (including shipping); (d) marine N_2O emissions for the year 2020 at 1 km^2 spatial resolution. Note that marine emissions are on a smaller scale than the other sectors and are not part of the NAEI. White areas indicate where emissions are zero.

Reports (NIRs) submitted annually to the United Nations Framework Convention on Climate Change (UNFCCC). Anthropogenic N_2O emissions of $72.6 \text{ Gg N}_2\text{O yr}^{-1}$ are reported in the NAEI for the year 2021 (Brown et al., 2023). This is around 4% of the UK's total carbon dioxide equivalent ($\text{CO}_{2,eq}$) GHG emissions. Agricultural N_2O emissions in the NAEI account for 70% of 2021 UK N_2O emissions, with $\sim 10\%$ of UK N_2O emissions attributed to fossil fuel combustion and fugitive emissions, and the remaining anthropogenic emissions coming from the waste and industrial sectors (Figure 1; Brown et al., 2023). Agricultural emissions are predominately from agricultural soils (57% of UK N_2O emissions) with the remaining agricultural N_2O emissions mostly from livestock manure management as well as indirect emissions from nitrogen runoff and leaching. A feature of the NAEI is that GHG fluxes are spatially distributed at 1 km^2 resolution for each SNAP (Selected Nomenclature for reporting of Air Pollutants) sector.

Under the 2008 Climate Change Act (UK Government, 2008) the UK has ambitious goals to achieve Net Zero GHG emissions by 2050. Interim targets ("Carbon Budgets") have been enacted, with the Fifth UK Carbon Budget requiring GHG emissions to be reduced to 57% of 1990 $\text{CO}_{2,eq}$ levels by 2030 (UK Committee on Climate Change, 2015). Current GHG emissions mitigation policy suggest UK N_2O emissions will remain approximately constant until 2030 (UK Department for Energy Security and Net Zero, 2022). Given the potential uncertainties in inventories, which are used to guide these policy scenarios, there is a need to independently monitor progress toward such targets.

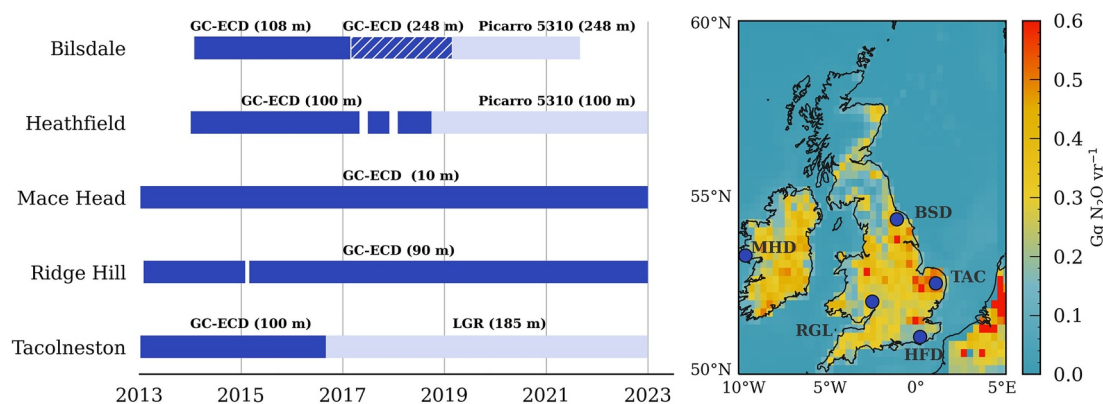


Figure 2. Summary of atmospheric N_2O mole fraction data used from the UK DECC network for 2013–2022. Instrument names and inlet heights (in brackets with “m” referring to meters above ground level) used for different periods are shown on the left. Gaps (white space) denote when measurements were unavailable. Shaded blue sections represent when gas chromatographs coupled to electron capture detectors (GC-ECD) were used, whereas sections shaded in lighter blue are when optical spectrometers were used. Hatched areas represent periods using GC-ECD measurements after a change in inlet height. Station locations are shown on the right in blue along with the May 2020 UKEM N_2O emissions regridged to match the atmospheric transport footprint resolution.

Atmospheric mole fraction measurements of trace gases can be used to evaluate emissions reported in national greenhouse gas inventories through inverse modeling. Atmospheric measurements are used in the inverse model to adjust bottom-up emissions through Bayesian inference. This approach has previously been used for deriving top-down N_2O emissions for the UK (Ganesan et al., 2015; Manning et al., 2011) and elsewhere (e.g., Nevison et al., 2018; Stell et al., 2022; Thompson et al., 2014). Previous studies found top-down emissions were approximately 13%–22% lower than those reported in the UK inventory at that time (2009 and 2012 UNFCCC reported emissions respectively for Manning et al., 2011; Ganesan et al., 2015) - the UK updates its entire bottom-up emissions inventory record each year (Figure S1 in Supporting Information S1). Top-down emissions for earlier than 2012 had relatively large uncertainties as atmospheric observations were only available from Mace Head station on the west coast of the Republic of Ireland (Figure 2). The establishment of the UK Deriving Emissions linked to Climate Change (DECC) network in 2012 for making continuous atmospheric trace gas measurements across the UK (Stanley et al., 2018; Stavert et al., 2019) has improved top-down emissions estimates. The UK DECC network provides a higher sensitivity to emissions across the UK and Republic of Ireland, leading to smaller top-down uncertainties (e.g., Lunt et al., 2021).

Ganesan et al. (2015), using atmospheric N_2O measurements from the UK DECC network with a hierarchical Bayesian inverse model (Ganesan et al., 2014), inferred average UK emissions of 101 (68–150) $\text{Gg N}_2\text{O yr}^{-1}$ for 2012–2014 and identified a pronounced seasonal cycle with an amplitude of $\sim 50 \text{ Gg N}_2\text{O yr}^{-1}$ peaking during the early summer. The observed seasonality was hypothesized to be due to agricultural applications of nitrogen-based fertilizers.

Seasonal changes in UK N_2O emissions are not captured in the UK NAEI inventory, which only produces annual estimates. To compare top-down and bottom-up seasonal cycles, temporal profiles derived from direct flux measurements and other data sources are used to downscale the annual NAEI N_2O emissions at a source sub-sector level to a monthly time resolution. These are combined with marine emissions from Lessin et al. (2020) for the surrounding seas in the UK Emissions Model (UKEM, previously referred to as “UKGHG”; Levy, 2020).

Here, we present results of monthly top-down UK N_2O emissions from 2013 to 2022 derived using two different Bayesian inverse models and compare these estimates to the UK NAEI and the downscaled monthly estimates from the UKEM. Compared to previous UK N_2O publications, we use observations from five stations in the UK DECC network (only three stations were available for Ganesan et al., 2015) and over a longer time period, resulting in better resolved emissions trends and seasonal patterns.

2. Data and Methods

2.1. Atmospheric Measurements

We use atmospheric N₂O mole fraction measurements from five UK DECC network stations (Stanley et al., 2018; Stavert et al., 2019) between 2013 and 2022. Tall-tower measurement stations in the UK DECC network sample ambient air from inlets mounted >90 m above ground level (agl) on telecommunications towers (Figure 2), and the coastal Mace Head (MHD) station measures closer to the surface at ~10 m agl. Atmospheric N₂O measurements from MHD, Tacolneston (TAC) and Ridge Hill (RGL) stations sampled across the entire 2013–2022 period, with Bilsdale (BSD) and Heathfield (HFD) becoming operational in 2014.

Both gas chromatograph coupled to electron capture detectors (GC-ECD) and optical-based instruments (Picarro G5310, LGR; Text S1) are used for measuring atmospheric N₂O mole fractions in the UK DECC network. Optical instruments are calibrated to the World Meteorological Organization (WMO)-X2006A scale (Hall et al., 2007) with samples averaged into ~1 min intervals. The GC-ECD instruments are calibrated to the Scripps Institution of Oceanography (SIO-16) scale and sample approximately every 10 min. A correction of –0.43 ppb is applied to N₂O measurements made on the SIO-16 scale to adjust these measurements to the WMO-X2006A calibration scale (Prinn et al., 2018).

At certain measurement stations (e.g., BSD) there are periods when concurrent GC-ECD and optical-based atmospheric N₂O measurements are available. In such cases, we use measurements from optical-based instruments in preference to those from the GC-ECD instruments, due to their greater precision and higher frequency. Measurements are always used from the highest air inlet available. Information about the instrumentation and inlet heights used for each of the stations are summarized in Figure 2, with the UK DECC network further described in Stanley et al. (2018) and Stavert et al. (2019).

Measurements were averaged over 4 hr periods and filtered to remove measurements that are more likely to be affected by local processes during times of stagnant air (e.g., Ganesan et al., 2015). Such meteorological conditions are unlikely to be accurately captured at the spatiotemporal resolution of the atmospheric transport model (Section 2.2) used in this work. Each inverse model uses a different approach for filtering atmospheric measurements during stagnant air conditions. Further details about the filtering approaches are provided in Text S2 in Supporting Information S1. A comparison of top-down emissions derived using the same inverse method with the different filtering approaches, and without any data filtering, is presented in Text S3 in Supporting Information S1.

Uncertainty in the atmospheric N₂O observations is quantified as the sum in quadrature of the instrument precision and observation variability in the 4 hr averaging period. Observation uncertainties were on average ~0.28 ppb for the GC-ECD instruments and ~0.21 ppb for the optical instruments across the respective periods shown in Figure 2.

2.2. Atmospheric Transport Model

The UK Met Office Lagrangian dispersion model: NAME (Numerical Atmospheric dispersion Modelling Environment; Jones et al., 2007) v7.2 was used to quantify the relationship between surface emissions and atmospheric mole fractions measured at each station in both inverse models (Section 2.3). “Footprints” of surface emission sensitivities were calculated from ensembles of particle back-trajectories in NAME. Each grid cell of the footprint describes the influence of emissions from that grid cell on the measured mole fractions at the measurement site at a certain time (Manning et al., 2011; Rigby et al., 2012).

Hourly footprints were calculated as described in Manning et al. (2021) with a ~25 × 25 km² (0.352° × 0.234°) spatial resolution over a model domain spanning approximately 98°W to 40°E and 11°N to 79°N using a 30 day integrated back-trajectory duration and particle release rate of 2 × 10⁴ hr^{–1}. Meteorological fields from the Met Office Unified Model (UM) underlie the footprints with hourly, high-resolution (up to ~1.5 km (0.0135° × 0.0135°) with 57 vertical levels up to ~12 km) UKV meteorological fields used for over the British Isles and three-hourly UM (0.1406° × 0.0938° with 59 vertical levels up to ~30 km) global meteorological fields used for the rest of the modeling domain. The mean NAME-modeled sensitivity of the UK DECC network to surface emissions has been previously shown in other UK studies (e.g., Lunt et al., 2021).

Footprints were combined with gridded a priori emissions (Section 2.4) to simulate atmospheric N₂O mole fraction enhancements at each measurement station.

2.3. Inversion Methodology

Two inverse models - InTEM (Inversion Technique for Emissions Modeling) and RHIME (Regional Hierarchical Inverse Modeling Environment) - were used for deriving top-down UK N₂O emissions and are described below. Whilst both inverse models follow a Bayesian framework the inverse methods differ in several aspects: in the calculation of baseline mole fractions; the treatment of model-data uncertainties; and the approach for calculating the posterior emissions. Both inverse models infer emissions for each calendar month assuming N₂O emissions are constant in each 1 month period of inference.

2.3.1. InTEM Inverse Model

InTEM is an established Bayesian inverse model (Arnold et al., 2018; Manning et al., 2011, 2021) developed by the UK Met Office that has been widely used for trace gas inversions of different species across different regions (e.g., Ganesan et al., 2020; Manning et al., 2021; Rigby et al., 2019). InTEM is also used by the UK Government for evaluating its nationally reported greenhouse gas emissions (Brown et al., 2022, 2023).

The InTEM framework minimizes the model-data mismatch constrained by observation uncertainties, model uncertainties, and a priori information and its associated uncertainties, which are assumed to be Gaussian. To prevent non-physical solutions, InTEM uses a non-negative least squares solver. The model-data uncertainty is calculated as the sum in quadrature of the observational uncertainty, baseline uncertainty and estimated model uncertainty. The observation uncertainty is defined as the sum in quadrature of the daily precision, and the variability of atmospheric measurements over a 4 hr period centered at the time of interest. The baseline uncertainty is defined by the goodness of fit of a fourth order polynomial fitted through the baseline mole fractions. The model uncertainty forms the largest contribution of the model-data uncertainty in InTEM and is calculated (for all trace gas species) by using the larger of: the mole fraction of the median pollution event over the year, or 10% of the mole fraction of the individual pollution event. InTEM also imposes a 12 hr temporal correlation and 100 km spatial correlation in its framework.

InTEM uses bottom-up gridded N₂O emissions (Section 2.4) and a time-varying mole fraction baseline as a priori constraints. The mole fraction baseline is derived using atmospheric N₂O measurements from Mace Head that are representative of the well-mixed northern hemispheric background. This baseline is derived using filters to minimize influences from populated regions, local sources, high altitudes and southerly latitudes (Manning et al., 2021). The mole fraction baseline is subsequently adjusted in the inversion by 11 values depending on the geographical direction and altitude from which the air enters the model domain (Arnold et al., 2018), along with the spatial distribution of N₂O emission values (Arnold et al., 2018; Manning et al., 2021). InTEM solves for posterior emissions in 100 scaling regions across its inversion domain. The scaling regions that cover Europe (30° W–42°E longitude and 29.3°N–77.3°N latitude) are not spatially fixed and are recalculated for each month. Scaling regions in the rest of the inversion domain are always spatially fixed. The geographical coverage of each scaling region in Europe is calculated from multiplying the mean footprint field with the converging estimated emissions field for each month. The inversion domain is split (with land and sea areas kept distinct in each scaling region) such that summing the grid cells in each scaling region yields approximately the same footprint-emissions value. Scaling regions closer to the measurement stations encompass fewer grid cells (and a smaller geographical area) than those much further from the UK which encompass larger geographical areas. There are approximately 20 scaling regions across the land component of the UK. An a priori emissions uncertainty of 80% of NAEI N₂O emissions is imposed for the UK. Both inverse models account for any small instrumental (or model-related) differences that might occur in the atmospheric measurements across the network by solving for a mole fraction bias (\pm) at each measurement station in each month. A prior mole fraction bias with mean of 0 ppb and 1σ uncertainty of 0.6 ppb is included for each station and subsequently solved for in the inversion. InTEM is further described in Manning et al. (2021); Arnold et al. (2018); Redington et al. (2023).

2.3.2. RHIME Inverse Model

RHIME (also previously referred to as “Bristol-MCMC”; Ganesan et al., 2014) has been frequently used for trace gas inversions of various atmospheric species across the globe (e.g., Ganesan et al., 2015; Say et al., 2021;

Western et al., 2022). Here, Bayesian inference using MCMC (Markov Chain Monte Carlo) is used to quantify a mean scaling (with confidence intervals) of a priori emissions across 193 scaling regions in the RHIME inversion domain that also matches the NAME model domain. Scaling regions are calculated as described for InTEM but with approximately 40 scaling regions covering the land component of the UK. An a priori emissions uncertainty of 17% of NAEI N₂O emissions is imposed for the UK. A scaling of boundary conditions on the four cardinal boundaries of the NAME domain is also derived in the inversion.

Boundary condition fields representing mole fractions along the edges of the NAME model domain are specified using CAMS (Copernicus Atmosphere Monitoring Service) v20r1 global inversion-optimized fluxes for each month. A scaling is calculated for each boundary in each 1 month period of inference to derive posterior boundary condition mole fractions. This ensures the CAMS data are not systematically underestimating or overestimating the baseline mole fractions at each of the measurement stations.

RHIME uses hyperparameters that characterize probability density functions (PDFs) of: the a priori emissions, the boundary condition mole fractions, the model-data covariances and the mole fraction bias terms. The RHIME framework allows uncertainties in the scaling parameters to be included in the model. The a priori scaling is sampled from a lognormal distribution $\sim LN(\mu = 0.346, \sigma = 0.693)$ and the model uncertainty from a uniform distribution bounded between 0.1 and 3.0. The model-data uncertainty is calculated as the sum in quadrature of the observational uncertainty and the model uncertainty - derived from the model hyperparameter. The mole fraction bias term is normally distributed with a mean of zero ppb and uncertainty of 0.6 ppb. Like Western et al. (2022) and Say et al. (2021), we use a No-U-Turn (NUTS) sampler (Hoffman & Gelman, 2014) for the a priori emissions and a slice sampler for estimating the model-data uncertainty. The samplers used a total 250,000 iterations (discarding the first 50,000) with two chains running in parallel. A Gelman-Rubin diagnostic is used to check for parameter convergence in both chains.

2.4. A Priori Emissions

The UKEM model (Levy, 2020) takes spatial data from the UK and Republic of Ireland inventories and processes them in a number of steps. These steps include: reprojection to a latitude-longitude grid, combining point- and area-based emissions, reconciling data from different sources into a single consistent classification scheme, rescaling to match national totals, back-projecting a time series of maps as inventories are updated annually, and adding in marine biogenic fluxes. For N₂O, marine biogenic fluxes from NEMO-ERSEM (the Nucleus for European Modeling of the Ocean model coupled with the European Regional Seas Ecosystem Model; Lessin et al., 2020) were used as the best available data on fluxes for the coastal sea around the UK.

Inventory data are only produced annually. However, emissions may vary over much shorter timescales. The annual-scale emissions are disaggregated in time in UKEM, to give the appropriate seasonal, day-of-week, and diurnal patterns. For some sectors, the variation in time is largely negligible (e.g., industry) or poorly known (e.g., LULUCF, waste), and these are represented as constant in time. For other sectors (agriculture, transport, energy), strong temporal patterns exist and can be characterized with activity data at a higher temporal resolution from a variety of sources (Levy et al., 2017).

For N₂O, the key sector is agriculture. The UKEM model uses activity data from the same process as the agricultural GHG inventory (Brown et al., 2023) but at a monthly resolution when available. For example, the timing of synthetic fertilizer application is estimated from the British Survey of Fertilizer Practice (<https://www.gov.uk/government/collections/fertiliser-usage>, Date of last access: 8 July 2024). The timing of N₂O emissions after application is estimated from existing data where fluxes have been measured in the field, generally using the closed static chamber technique. Typically, most of the emission occurs within only a few weeks of application (Levy et al., 2017). This produces a pronounced peak in the late spring, closely following the pattern in the application of synthetic fertilizer. The spatial distribution follows the distribution of cropland, where fertilizer inputs are highest (Figure 1). An additional source is the mineralization of degrading peat soils in the Fenland areas in south-east England, though the magnitude of this is very uncertain.

Emissions from the marine sector are generally highest in the coastal zone, where inputs from rivers produce higher nitrogen concentrations. However, even near the coast, marine emissions are around ten times smaller than land emissions (Figure 1), and although they peak during summer, their influence on the overall pattern is

relatively small. At times, the modeled marine fluxes show net N₂O uptake, but only in a small region in the north-west of the domain.

As UKEM N₂O monthly emissions are only available for the UK and Republic of Ireland, 0.1° × 0.1° monthly anthropogenic emissions from EDGAR (Emissions Database for Global Atmospheric Research; Crippa et al., 2021) v6.0 are used for the rest of the modeling domain. Version 6.0 is used because monthly N₂O emissions are not currently available in the latest version (v7.0) of EDGAR. We “regrid” emissions data to match the NAME footprint spatial resolution and domain using a mass-conservative approach. As gridded emissions were only available for each month in 2013–2020, 2020 emissions were used as the a priori estimate for the 2021 and 2022 inversions.

Two sets of a priori emissions were used in the inversions. The first used the monthly resolved emissions and the second used annual emissions, which are constant across each year. This provides an additional means of diagnosing whether any seasonal trends in the posterior emissions are driven by atmospheric measurements or by the a priori emissions.

2.5. Optimization of Sectoral Seasonal Profiles

We are interested in comparing the UK top-down (derived using the inverse models; Section 2.3) and bottom-up (modeled in UKEM; Section 2.4) seasonal emissions profiles.

To investigate which N₂O emissions sources could be driving seasonal differences we identified key agricultural sub-sectors that exhibit seasonal cycles in the UK. These are: synthetic fertilizer usage, and manure management practices relating to: cattle during times they are housed (“cattle housing”), cattle during times of grazing (“cattle grazing”), the spreading of cattle manure, the spreading of poultry manure, and the spreading of digestate. Bottom-up emissions from all remaining N₂O sources are aggregated together. Each of these agricultural sub-sectors has a distinct temporal seasonal profile in the bottom-up UKEM emissions. However, varying the spatial distributions of the different sub-sector fluxes independently is a more complex problem, and not currently feasible with the inventory data available.

We optimize the 2013–2022 averaged UKEM sub-sector emissions profiles to the averaged top-down seasonal emissions cycles - derived using InTEM and RHIME - to investigate which bottom-up emissions sources could be leading to differences with the top-down seasonal cycles.

We use a Bayesian approach to calculate the scale factors for each bottom-up sub-sector that minimizes the mismatch with the average top-down seasonal cycles. The posterior scale factors, \mathbf{X}_{post} , for each of the seven bottom-up sub-sector seasonal profiles are calculated using:

$$\mathbf{X}_{post} = \mathbf{X}_{prior} + (\mathbf{Q}_{prior} \mathbf{H}^T) (\mathbf{H} \mathbf{Q}_{prior} \mathbf{H}^T + \mathbf{R})^{-1} (\mathbf{Y} - \mathbf{H} \mathbf{X}_{prior}), \quad (1)$$

with associated covariance:

$$\mathbf{Q}_{post} = \mathbf{Q}_{prior} - (\mathbf{Q}_{prior} \mathbf{H}^T) (\mathbf{H} \mathbf{Q}_{prior} \mathbf{H}^T + \mathbf{R})^{-1} \mathbf{H} \mathbf{Q}_{prior}. \quad (2)$$

Here, \mathbf{X}_{prior} is a 7 × 1 matrix with elements of value one denoting the a priori scale factors for each UKEM emissions sub-sector. \mathbf{H} is a 12 × 7 matrix representing the monthly sub-sector UKEM seasonal emissions profiles (in Gg N₂O yr⁻¹). \mathbf{Y} is a 12 × 1 matrix representing the average top-down seasonal emissions (in Gg N₂O yr⁻¹) with associated uncertainties (in Gg N₂O yr⁻¹) captured in \mathbf{R} . Matrix \mathbf{R} is a 12 × 12 diagonal matrix where each element is the corresponding monthly 1σ value of the top-down seasonal emissions cycle. The uncertainty of the scale factors for each of the UKEM seasonal profiles are captured in \mathbf{Q} which is a 7 × 7 diagonal matrix with elements of value one denoting uncertainties of 100% on each of the bottom-up sub-sectors.

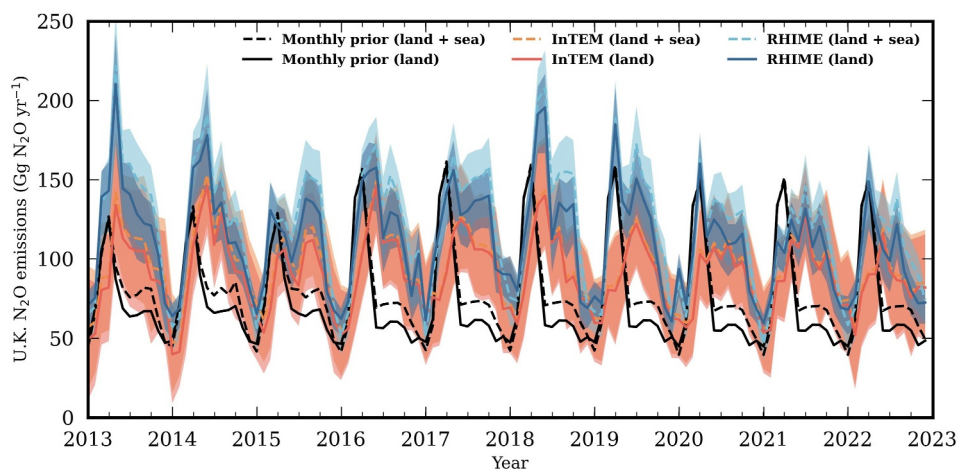


Figure 3. Time series of a priori and posterior monthly N_2O emissions for the UK. Mean monthly posterior emissions from InTEM (red) and RHIME (blue) for the land component of the UK (solid line) and the land plus surrounding seas of the UK (dashed line) with corresponding monthly a priori emissions in black. Shaded regions correspond to the 68% confidence interval ranges.

3. Results

3.1. Emissions and Trends in N_2O (2013–2022)

For 2013–2020, the NAEI reported average UK N_2O emissions of 73.9 ± 1.7 (1σ) $Gg\ N_2O\ yr^{-1}$. Over 2013–2022, average top-down UK N_2O emissions of 90.5 ± 23.0 (1σ) $Gg\ N_2O\ yr^{-1}$ and 111.7 ± 32.1 (1σ) $Gg\ N_2O\ yr^{-1}$ were inferred by InTEM and RHIME, respectively (Figure 3, Table 1).

Table 1

Summary of 2013–2022 Mean UK Posterior and a Priori N_2O Emissions and Their Differences Reported With 1σ Uncertainty. “Monthly” and “Annual” Reference Posterior Emissions Derived Using the Monthly UKEM and Annual NAEI Emissions, Respectively

Inversion setup	InTEM		RHIME		UKEM
	Monthly	Annual	Monthly	Annual	Monthly
Land emissions ($Gg\ N_2O\ yr^{-1}$)	90.5 ± 23.0	90.5 ± 23.0	111.7 ± 32.1	116.1 ± 26.9	73.9 ± 31.9
Marine emissions ($Gg\ N_2O\ yr^{-1}$)	4.2 ± 2.1	4.2 ± 2.2	8.1 ± 10.5	17.9 ± 29.9	6.4 ± 6.9
Land plus marine emissions ($Gg\ N_2O\ yr^{-1}$)	94.7 ± 23.1	94.7 ± 23.0	119.8 ± 37.1	129.7 ± 36.0	80.1 ± 30.8
Mean Posterior - A Priori Emissions					
Land					
Percentage difference	$22.5\% \pm 50.1\%$	$18.5\% \pm 25.5\%$	$51.2\% \pm 51.9\%$	$51.9\% \pm 23.3\%$	-
$Gg\ N_2O\ yr^{-1}$ difference	16.6 ± 8.3	14.1 ± 3.6	37.8 ± 19.6	39.7 ± 9.2	-
Marine					
Percentage difference	$-65.6\% \pm 18.8\%$	$55.3\% \pm 271\%$	$26.6\% \pm 68.6\%$	$49.2\% \pm 314\%$	-
$Gg\ N_2O\ yr^{-1}$ difference	-2.2 ± 0.4	-3.4 ± 5.8	1.7 ± 1.2	5.9 ± 12.6	-
Land plus marine					
Percentage difference	$18.2\% \pm 45.5\%$	$12.6\% \pm 24.4\%$	$49.6\% \pm 49.4\%$	$54.3\% \pm 27.8\%$	-
$Gg\ N_2O\ yr^{-1}$ difference	14.6 ± 6.6	10.6 ± 2.6	39.7 ± 19.6	45.6 ± 12.7	-

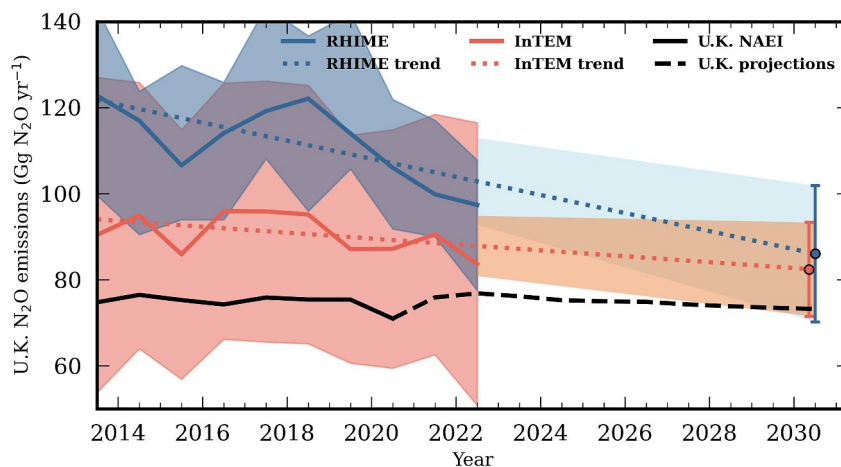


Figure 4. Annual top-down UK N₂O emissions from InTEM (red) and RHIME (blue) along with the linear trends for 2013–2022 that are extrapolated to 2030, with 2030 values indicated by circular markers. Shaded areas and error bars denote the 1 σ range. Current UK NAEI emissions and UK DESNZ projected emissions are shown in black.

Top-down UK N₂O emissions were generally higher than their corresponding bottom-up UKEM/NAEI emissions across the 10 year period spanning January 2013 to December 2022 (Figure 3, Table 1). On average, top-down emissions from RHIME were 38.0 ± 32.6 (1 σ) Gg N₂O yr⁻¹ (51.2%) higher than the bottom-up estimates, and InTEM was 16.8 ± 37.4 (1 σ) Gg N₂O yr⁻¹ (22.4%) higher. Whilst RHIME posterior emissions are on average 21.2 ± 19.9 (1 σ) Gg N₂O yr⁻¹ higher than the InTEM posterior emissions, there are overlapping 68% confidence intervals (CI) for most of the inversion period. The InTEM and RHIME top-down emissions are statistically well-correlated ($R^2 = 0.86$, $p < 0.01$). We discuss reasons for differences between InTEM and RHIME top-down emissions in Texts S4 and S5 in Supporting Information S1.

We find an average of 5% of UK top-down emissions originate from the surrounding seas (Figure 3; Table 1), whereas a priori emissions estimate 8% of UK N₂O emissions arise from the marine sector. InTEM infers that marine emissions should on average be lower than the bottom-up estimates whereas RHIME infers the opposite (Table 1). Previous studies have highlighted that UK DECC stations are less sensitive to offshore emissions (Lunt et al., 2021) and as marine emissions form a small proportion of UK N₂O emissions we limit our analysis to land-based emissions.

We determine the RHIME and InTEM emissions trend over 2013–2022 by applying a linear regression to the annual totals. Across this period, a mean negative trend of -2.10 ± 0.72 (1 σ) Gg N₂O yr⁻² (p val = 0.01, $R^2 = 0.52$) was calculated for RHIME top-down emissions and -0.68 ± 0.48 (1 σ) Gg N₂O yr⁻² (p val = 0.20, $R^2 = 0.19$) for InTEM top-down emissions (Figure 4). Figure 4 shows that, comparatively, the NAEI N₂O emissions remain relatively constant across this period.

The UK Government Department for Energy Security and Net Zero (DESNZ) produces GHG emissions projections based on current UK NAEI emissions and existing/near-finalized UK emissions mitigation policies (UK Department for Business Energy and Industrial Strategy, 2022). Projected UK N₂O emissions from 2022 to 2030 are shown in Figure 4 and remain relatively constant at around 70 Gg N₂O yr⁻¹. Extrapolating the InTEM and RHIME 2013–2022 emissions trends finds projected emissions of 82.3 ± 10.9 (1 σ) Gg N₂O yr⁻¹ and 86.5 ± 16.7 (1 σ) Gg N₂O yr⁻¹, respectively, for the year 2030 (Figure 4).

3.2. Seasonal Cycles

Pronounced seasonal cycles are observed in the top-down emissions with seasonal highs occurring during the late spring and seasonal lows during the winter (Figure 5). We find top-down seasonal cycles are insensitive to the seasonality in the prior. Figure S3 in Supporting Information S1 shows a comparison between posterior emissions that used a priori monthly UKEM emissions that either included or excluded a seasonal cycle. A pronounced seasonal peak is always derived in the top-down emissions. There is strong agreement between the two sets of posterior emissions (Table 1), indicating that the derived seasonal cycle is primarily observation driven.

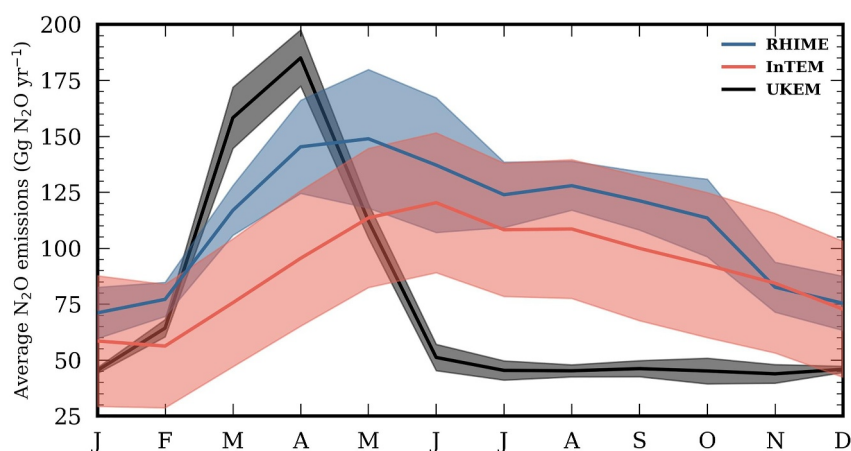


Figure 5. Average seasonal emissions profile across 2013–2022 with shaded regions denoting the 1σ standard deviation in emissions for each month.

In certain years there is a clearly identifiable springtime peak, as modeled in the bottom-up UKEM emissions, and a secondary, smaller peak occurring later in the year. From 2020 onwards, the second seasonal peak (occurring in late summer) is not as distinct from the primary seasonal peak (occurring late spring/early summer) as in the 2015–2019 seasonal cycles (Figure 3).

The average seasonal emissions from 2013 to 2022 for top-down and bottom-up emissions are shown in Figure 5. In UKEM, the modeled springtime seasonal peak rapidly declines. This is not seen in the top-down emissions, which instead fall more slowly. Additionally, the secondary peak that is sometimes seen in the top-down emissions seasonal cycles (Figure 3) is not seen in UKEM. We find there are differences between the average InTEM and RHIME seasonal cycles. The occurrence of a late-summer/autumnal peak is less distinctive in InTEM than in RHIME, with the average InTEM seasonal cycle appearing more prolonged. The shaded regions in Figure 5, which denote the 1σ standard deviation in emissions for each month across 2013–2022, indicate variability in the RHIME seasonal cycle is less than in InTEM for most months. Whilst the variability in the InTEM seasonal cycle is similar each month (Figure 5), the variability between April–July in RHIME, when the seasonal maximum occurs, is much larger than in other months.

3.3. Uncertainty Analysis

Model-data uncertainties are defined as the sum in quadrature of the observational uncertainty, and model uncertainty for RHIME (Section 2.3.2), and the model uncertainty plus baseline uncertainty for InTEM (Section 2.3.1). In RHIME, the model uncertainty is solved for in the inversion whereas InTEM uses a proportion of the magnitude of the simulated pollution events for the model uncertainty (Section 2.3.1). Median model-data uncertainties are less than one ppb in both models, with InTEM uncertainties being nearly four times larger than the posterior values from RHIME. These differences are also reflected in the 68% confidence interval ranges for each station (Figure 6a), which are generally larger in InTEM. Differences in model-data uncertainties are attributed to differences in how the model uncertainty is attributed in InTEM and in RHIME and the way model uncertainties are defined in InTEM compared to RHIME.

The InTEM and RHIME inversions account for any small instrumental (or model-related) differences that might occur by solving for a mole fraction bias at each measurement station in each month. The median values with their 68% confidence intervals for each measurement station in InTEM and in RHIME are shown in Figure 6b. The median bias values from each inversion are typically within ± 0.2 ppb at each station; similar to the measurement precision of the instruments (Section 2.1). However, median values differ by around 0.1 ppb between InTEM and RHIME with the largest discrepancies occurring at Bilsdale and Ridge Hill stations. The large, overlapping 68% confidence intervals indicate considerable variability in the biases that are solved in the monthly inversions. The posterior biases underscore that instrument or model-related differences exist across the UK DECC network for N_2O at a magnitude comparable to the N_2O observation uncertainty. The high-variability in the mole fraction bias values suggests that these instrument-related differences are not constant in time and should be accounted for in

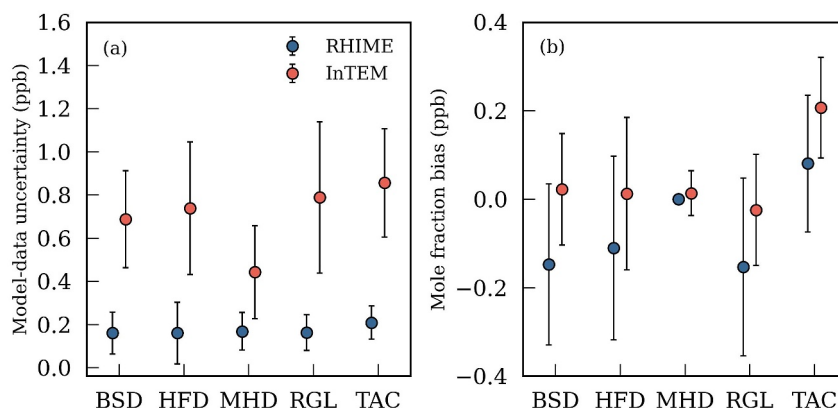


Figure 6. (a) Mean model-data uncertainties for InTEM (red) and RHIME (blue) for each of the measurement stations with error bars denoting the 68% confidence intervals. (b) Inverse model posterior mole fraction bias median and 68% confidence intervals for each of the stations calculated in InTEM (red) and RHIME (blue).

N_2O inverse modeling studies using measurements from the UK DECC network. This has also been seen in other measurement networks (e.g., Thompson et al., 2011; Thompson et al., 2014).

3.4. Posterior UKEM Sub-Sector Emissions Seasonal Profiles

Figure 7a shows the 2013–2022 averaged UKEM seasonal cycles of six N_2O agricultural emissions sub-sectors (Section 2.5) with the remaining land-based N_2O emissions aggregated under “Other”. The pronounced springtime peak is driven by synthetic fertilizer emissions with some contribution from manure management sub-sectors.

As shown in Figure 5, there are clear differences between the average bottom-up and top-down seasonal cycles for UK N_2O emissions across 2013–2022. To investigate what could be driving these differences, we use Bayesian inference (Section 2.5) to calculate mean scale factors for each UKEM sub-sector that optimize the fit to the observed average seasonal cycle. The seasonal profiles of the individual sub-sectors from the UKEM are preserved.

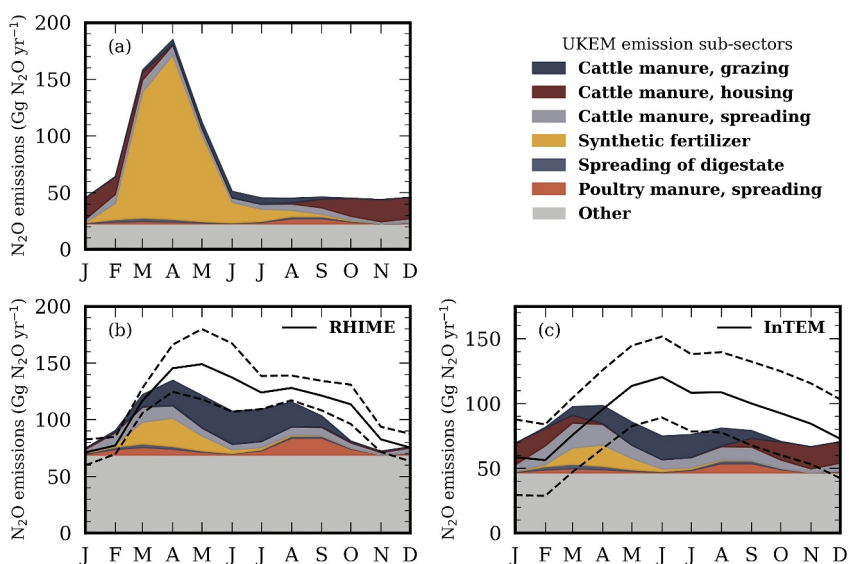


Figure 7. 2013–2022 averaged N_2O seasonal emissions profiles. (a) Sub-sector emissions profiles as modeled in UKEM. Averaged RHIME and InTEM top-down seasonal emissions (solid lines) and 68% CI (dashed lines) with corresponding mean optimized (posterior) sub-sector emissions are shown in (b) and (c), respectively.

Table 2
Mean and 1σ Range of UKEM a Priori Sub-Sector Emissions and Respective RHIME and InTEM Optimized Sub-Sector Emissions in $\text{Gg N}_2\text{O yr}^{-1}$

UKEM emissions sub-sector	UKEM emissions ($\text{Gg N}_2\text{O yr}^{-1}$)	RHIME-optimized emissions ($\text{Gg N}_2\text{O yr}^{-1}$)	InTEM-optimized emissions ($\text{Gg N}_2\text{O yr}^{-1}$)	RHIME-optimized scale factor	InTEM-optimized scale factor
Cattle manure, grazing	2.50 ± 2.34	12.7 ± 12.0	7.96 ± 7.47	5.12 ± 1.51	3.19 ± 1.61
Cattle manure, housing	8.69 ± 8.05	0.51 ± 0.47	7.62 ± 7.05	0.05 ± 0.56	0.87 ± 0.87
Cattle manure, spreading	5.28 ± 2.50	6.64 ± 3.15	9.65 ± 4.57	1.26 ± 1.28	1.83 ± 1.59
Synthetic fertilizer	32.0 ± 45.9	5.50 ± 8.30	3.61 ± 5.41	0.17 ± 0.12	0.11 ± 0.20
Spreading of digestate	1.40 ± 0.89	1.39 ± 0.89	1.55 ± 0.98	1.00 ± 1.70	1.11 ± 1.74
Poultry manure, spreading	1.48 ± 1.42	5.01 ± 4.83	2.42 ± 2.33	3.41 ± 1.53	1.64 ± 1.73
Other	22.6 ± 0.0	68.9 ± 0.0	46.5 ± 0.0	3.05 ± 0.43	2.05 ± 0.49

Note. Mean and 1σ uncertainty in the posterior scale factors for each UKEM emissions sub-sector when optimized to the average InTEM and RHIME seasonal cycles.

Figures 7b and 7c show the optimized (posterior) sub-sectors that produce the best match with the averaged seasonal cycles from RHIME and InTEM, respectively. We find the optimized fits do not generally have good agreement with the RHIME ($R^2 = 0.86$, $p|t| < 0.01$) and InTEM ($R^2 = 0.11$, $p|t| = 0.7$) seasonal cycles. Despite the large uncertainties in RHIME and InTEM there are certain months where the optimized bottom-up seasonal cycle does not fall within the RHIME/InTEM uncertainty. The fit to InTEM is generally worse than for RHIME, which could be due to the absence of two peaks in its average seasonal cycle and larger emissions uncertainties than RHIME.

For RHIME and InTEM, a decrease in synthetic fertilizer emissions and an increase in “Other” emissions are inferred in the posterior seasonal profiles (Figure 7, Table 2). An increase in emissions related to cattle manure during times of grazing and the spreading of poultry manure could explain some of the seasonal differences with RHIME-inferred emissions in the latter half of the year. Whereas an increase in emissions related to the spreading of digestate, cattle manure during times of grazing and housing could explain seasonal differences with InTEM-inferred emissions for the latter half of the year.

For January to April, there are only small differences between the RHIME/InTEM and optimized UKEM sub-sector emissions. After April, there is a larger mismatch between these seasonal cycles. This mismatch could be attributed to retaining the seasonal profiles of each UKEM emissions sub-sectors, which could have time-correlated uncertainties.

4. Discussion

Continuous atmospheric N_2O measurements from the UK and Republic of Ireland were used in InTEM and RHIME inverse models to derive top-down UK N_2O emissions and their trends over 2013–2022. Mean posterior UK terrestrial emissions from InTEM and RHIME over 2013–2022 were 90.5 ± 23.0 (1σ) $\text{Gg N}_2\text{O yr}^{-1}$ and 111.7 ± 32.1 (1σ) $\text{Gg N}_2\text{O yr}^{-1}$, respectively. The two inverse models inferred very different negative (and not statistically significant) trends of -0.68 ± 0.48 $\text{Gg N}_2\text{O yr}^{-2}$ and -2.10 ± 0.72 $\text{Gg N}_2\text{O yr}^{-2}$, respectively. However, it is unclear what could be driving a negative trend in the top-down emissions as the NAEI/UKEM sub-sector estimates do not have statistically significant trends over this period. Reconciling InTEM-RHIME discrepancies is important for accurately informing on the UK’s progress to meet GHG emissions mitigation targets. However, firm conclusions on the UK’s progress should not be drawn from the extrapolated trends presented in Figure 4. The sensitivity results presented in Text S4 in Supporting Information S1 suggest InTEM-RHIME discrepancies could be attributed to the different treatment of background mole fractions in each model.

We find that the top-down emissions are close to the 2012–2014 UK emissions estimates of 101 (68–150) $\text{Gg N}_2\text{O yr}^{-1}$ reported by Ganesan et al. (2015) and are approximately 22%–51% higher than the bottom-up N_2O emissions reported in NAEI. This discrepancy is higher than the 13%–22% differences between previously reported top-down and bottom-up estimates for the UK (Ganesan et al., 2015; Manning et al., 2011). However, we find the

inventory emissions are lower than the top-down emissions whereas previous UK N₂O studies found inventory emissions at that time were higher. The UK emissions inventory updates the entire record each year. Revisions to the UK's N₂O emissions are reflected in the UK's NIR submitted to the UNFCCC, which, for 2022, reported smaller N₂O emissions than were used as the a priori estimates in Ganesan et al. (2015) and Manning et al. (2011) at the time. Average differences of 22%–51% between top-down and bottom-up UK N₂O emissions underscore that there are still large uncertainties in UK N₂O emissions.

Similar to previous regional N₂O studies (e.g., Ganesan et al., 2015; Jeong et al., 2012; Nevison et al., 2018; Wagner-Riddle et al., 2017) we observe a pronounced seasonal cycle in the top-down N₂O emissions with a large springtime peak. We also observe a secondary peak in the late summer and/or a prolonged decay in the spring peak, which has not been previously observed in the UK. The observed seasonal patterns are likely to be driven by agricultural sources since the timings of these peaks are broadly consistent each year but climatic patterns could also have an influence. Top-down N₂O emissions in California, USA suggest the higher N₂O emissions observed during spring are linked to the application of fertilizers (Jeong et al., 2012, 2018; Xiang et al., 2013). Nevison et al. (2018) observed a dual seasonal maxima in top-down emissions from 2008 to 2014 in the USA with a spring peak attributed to fertilizer applications and a late winter peak attributed to freeze-thaw effects (e.g., Wagner-Riddle et al., 2017). Higher average winter temperatures in the UK and the timing of the second peak make it unlikely for freeze-thaw effects to be a driver of seasonal variations of N₂O emissions in the UK. Recent N₂O flux measurements over different terrestrial ecosystems in the UK found inconsistent seasonal patterns of total N₂O emissions across different land use types (Sgouridis & Ullah, 2017). This further suggests that seasonal variations with a springtime peak previously observed in the UK are driven by agricultural sources. However, environmental drivers such as precipitation and surface temperature also influence the magnitude and timing of agricultural N₂O emissions (Levy et al., 2017; Skiba et al., 2012).

We find the agreement between the average top-down and bottom-up seasonal cycles could be improved by reducing UKEM synthetic fertilizer N₂O emissions by an average of 27 Gg N₂O yr⁻¹ and increasing N₂O emissions from certain types of manure management - spreading of digestate and cattle manure during times of grazing and cattle housing - by an average of 4.9 Gg N₂O yr⁻¹. The optimizations also indicate the largest emissions increases (~34 Gg N₂O yr⁻¹) are from the aggregated sub-sectors that do not exhibit seasonal cycles. Modeling the temporal changes of manure management N₂O emissions is challenging as livestock waste management systems vary between sites and over time with little information available about their management practices (Chang et al., 2004). Fixing the temporal profiles of sub-sector emissions in the optimization could contribute to the top-down bottom-up seasonal cycle mismatch indicating there are uncertainties in the timings of N₂O emissions which require investigating. It is also probable the top-down and bottom-up seasonal cycle mismatch could be attributed to several other sources - such as missing emissions from NH₃ deposition - but this requires further investigation.

Whilst we find top-down emissions from InTEM and RHIME are well-correlated ($R^2 = 0.86$, $p|t| < 0.01$) there are differences in the magnitude and seasonal variations of N₂O emissions and uncertainties. Discrepancies between InTEM and RHIME most likely arise from differences in the baseline mole fractions and the treatment of model-data uncertainties. We find an average difference of 0.18 ± 0.22 (1 σ) ppb between the boundary condition mole fractions (Text S4 in Supporting Information S1). Furthermore, we find that redefining the model error in RHIME and solving for emissions using fixed InTEM posterior baseline mole fractions reduces the InTEM-RHIME top-down emissions mismatch (Text S5 in Supporting Information S1). A lower mole fraction baseline would lead to higher emissions being derived in the inversion.

The results from these long-term UK atmospheric N₂O measurements from a dense measurement network demonstrate that they can be used for effective evaluation of regional N₂O emissions by using inverse modeling. Understanding of differences between top-down and bottom-up N₂O emissions could be enhanced by comparing top-down emissions derived using a different atmospheric transport model with different underlying meteorological fields. Further long-term flux measurements of N₂O emissions sources could also provide additional constraints on the seasonal discrepancies observed between the average top-down and bottom-up seasonal cycles.

5. Conclusions

This study presents 10 years of top-down N₂O emissions derived using atmospheric measurements from across the UK and Republic of Ireland. Posterior emissions from both InTEM and RHIME inverse models find average

UK emissions of 90.5 ± 23.0 Gg N_2O yr^{-1} and 111.7 ± 32.1 Gg N_2O yr^{-1} , respectively across 2013–2020 which are $\sim 22.5\% \pm 50.1\%$ and $\sim 51.2\% \pm 51.9\%$ higher than estimated in the UK National Atmospheric Emissions Inventory, respectively. Average differences between the top-down and UKEM bottom-up seasonal patterns could be explained by decreasing synthetic fertilizer emissions by an average of 27 Gg N_2O yr^{-1} , and increasing N_2O manure management emissions (from cattle manure during grazing and housing) by an average of 4.9 Gg N_2O yr^{-1} . However, we find large uncertainties associated with the posterior scaling factors for the agricultural seasonal emissions profiles.

Data Availability Statement

Atmospheric measurements of N_2O used in this work are available from the CEDA Archive (O’Doherty et al., 2020) [Dataset]: <https://data.ceda.ac.uk/badc/uk-decc-network/data/n2o/v23.08>. A doi for this data is currently being assigned. Top-down emissions from RHIME and InTEM are available from (Saboya et al., 2024) [Dataset]. Python scripts used for data analysis are available for use in https://github.com/EricSaboya/uk_n2o.

References

- Arnold, T., Manning, A. J., Kim, J., Li, S., Webster, H., Thomson, D., et al. (2018). Inverse modelling of CF_4 and NF_3 emissions in east asia. *Atmospheric Chemistry and Physics*, 18, 13305–13320. <https://doi.org/10.5194/acp-18-13305-2018>
- Brown, P., Cardenas, L., Choudrie, S., Vento, S. D., Karagianni, E., MacCarthy, J., et al. (2022). UK greenhouse gas inventory 1990 to 2020: Annual report for submission under the framework convention on climate change. *Technical Reports Series*.
- Brown, P., Cardenas, L., Vento, S. D., Karagianni, E., MacCarthy, J., Mullen, P., et al. (2023). UK greenhouse gas inventory, 1990 to 2021 annual report for submission under the framework convention on climate change. *Tech. Rep. UK Department for Energy Security and Net Zero*.
- Chang, Y. H., Scrimshaw, M. D., & Lester, J. N. (2004). IPCC good practice guidance and uncertainty management in national greenhouse gas inventories. *Technical Reports Series*, 25.
- Crippa, M., Guizzardi, D., Solazzo, E., Muntean, M., Schaaf, E., Monforti-Ferrario, F., et al. (2021). GHG emissions of all world countries - 2021 report. *Technical Reports Series*.
- Ganesan, A. L., Manizza, M., Morgan, E. J., Harth, C. M., Kozlova, E., Lueker, T., et al. (2020). Marine nitrous oxide emissions from three eastern boundary upwelling systems inferred from atmospheric observations. *Geophysical Research Letters*, 47(14). <https://doi.org/10.1029/2020GL087822>
- Ganesan, A. L., Manning, A. J., Grant, A., Young, D., Oram, D. E., Sturges, W. T., et al. (2015). Quantifying methane and nitrous oxide emissions from the UK and Ireland using a national-scale monitoring network. *Atmospheric Chemistry and Physics*, 15(11), 6393–6406. <https://doi.org/10.5194/acp-15-6393-2015>
- Ganesan, A. L., Rigby, M., Zammit-Mangion, A., Manning, A. J., Prinn, R. G., Fraser, P. J., et al. (2014). Characterization of uncertainties in atmospheric trace gas inversions using hierarchical bayesian methods. *Atmospheric Chemistry and Physics*, 14(8), 3855–3864. <https://doi.org/10.5194/acp-14-3855-2014>
- Hall, B. D., Dutton, G. S., & Elkins, J. W. (2007). The NOAA nitrous oxide standard scale for atmospheric observations. *Journal of Geophysical Research*, 112(D9). <https://doi.org/10.1029/2006JD007954>
- Hoffman, M. D., & Gelman, A. (2014). The no-u-turn sampler: Adaptively setting path lengths in Hamiltonian Monte Carlo. *Journal of Machine Learning Research*, 15.
- Jeong, S., Newman, S., Zhang, J., Andrews, A. E., Bianco, L., Dlugokencky, E., et al. (2018). Inverse estimation of an annual cycle of California’s nitrous oxide emissions. *Journal of Geophysical Research: Atmospheres*, 123(9), 4758–4771. <https://doi.org/10.1029/2017JD028166>
- Jeong, S., Zhao, C., Andrews, A. E., Dlugokencky, E. J., Sweeney, C., Bianco, L., et al. (2012). Seasonal variations in N_2O emissions from central California. *Geophysical Research Letters*, 39(16). <https://doi.org/10.1029/2012GL052307>
- Jones, A., Thomson, D., Hort, M., & Devenish, B. (2007). The UK met office’s next-generation atmospheric dispersion model. *Name iii*. In, 580–589. Springer US. https://doi.org/10.1007/978-0-387-68854-1_62
- Lessin, G., Polimene, L., Artioli, Y., Butenschön, M., Clark, D. R., Brown, I., & Rees, A. P. (2020). Modeling the seasonality and controls of nitrous oxide emissions on the northwest european continental shelf. *Journal of Geophysical Research: Biogeosciences*, 125(6). <https://doi.org/10.1029/2019JG005613>
- Levy, P. (2020). Greenhouse gas fluxes from the UK (UKGHG/UKEM). [Software]. Retrieved from <https://github.com/NERC-CEH/ukghg/>
- Levy, P., Cowan, N., van Oijen, M., Famulari, D., Drewer, J., & Skiba, U. (2017). Estimation of cumulative fluxes of nitrous oxide: Uncertainty in temporal upscaling and emission factors. *European Journal of Soil Science*, 68(4), 400–411. <https://doi.org/10.1111/ejss.12432>
- Lunt, M. F., Manning, A. J., Allen, G., Arnold, T., Bauguitte, S. J.-B., Boesch, H., et al. (2021). Atmospheric observations consistent with reported decline in the UK’s methane emissions (2013–2020). *Atmospheric Chemistry and Physics*, 21, 16257–16276. <https://doi.org/10.5194/acp-21-16257-2021>
- Manning, A. J., O’Doherty, S., Jones, A. R., Simmonds, P. G., & Derwent, R. G. (2011). Estimating UK methane and nitrous oxide emissions from 1990 to 2007 using an inversion modeling approach. *Journal of Geophysical Research*, 116(D2), 1–19. (printed). <https://doi.org/10.1029/2010JD014763>
- Manning, A. J., Redington, A. L., Say, D., O’Doherty, S., Young, D., Simmonds, P. G., et al. (2021). Evidence of a recent decline in UK emissions of hydrofluorocarbons determined by the InT inverse model and atmospheric measurements. *Atmospheric Chemistry and Physics*, 21(16), 12739–12755. <https://doi.org/10.5194/acp-21-12739-2021>
- Nevison, C., Andrews, A., Thoning, K., Dlugokencky, E., Sweeney, C., Miller, S., et al. (2018). Nitrous oxide emissions estimated with the carbontracker-Lagrange north american regional inversion framework. *Global Biogeochemical Cycles*, 32(3), 463–485. <https://doi.org/10.1002/2017GB005759>
- O’Doherty, S., Say, D., Stanley, K., Spain, G., Arnold, T., Rennick, C., et al. (2020). UK DECC (deriving emissions linked to climate change) network. [Dataset]. Retrieved from <http://catalogue.ceda.ac.uk/uuid/f5b38d1654d84b03ba79060746541e4f>. Centre for Environmental Data Analysis

Acknowledgments

ES, ALG and MR were supported by NERC Highlight Topic Detection and Attribution of Regional Emissions in the UK (DARE-UK, NE/S004211/1). Thank you to Ray Weiss and Chris Harth of SIO for providing the measurement calibration standards. Thank you to Gennadi Lessin of Plymouth Marine Laboratory for running NEMO-ERSEM simulations used as the marine outputs. Thank you to Esmé Curtis for proofreading the article.

- Prinn, R. G., Weiss, R. F., Arduini, J., Arnold, T., Dewitt, H. L., Fraser, P. J., et al. (2018). History of chemically and radiatively important atmospheric gases from the advanced global atmospheric gases experiment (age). *Earth System Science Data*, *10*(2), 985–1018. <https://doi.org/10.5194/essd-10-985-2018>
- Redington, A. L., Manning, A. J., Henne, S., Grazioli, F., Western, L. M., Arduini, J., et al. (2023). Western european emission estimates of cfc-11, cfc-12 and ccl4 derived from atmospheric measurements from 2008 to 2021. *Atmospheric Chemistry and Physics*, *23*(13), 7383–7398. <https://doi.org/10.5194/acp-23-7383-2023>
- Ricardo Energy and Environment. (2019). UK emission mapping methodology 2017. (Tech. Rep.).
- Rigby, M., Manning, A. J., & Prinn, R. G. (2012). The value of high-frequency, high-precision methane isotopologue measurements for source and sink estimation. *Journal of Geophysical Research*, *117*(D12), 1–14. <https://doi.org/10.1029/2011JD017384>
- Rigby, M., Park, S., Saito, T., Western, L. M., Redington, A. L., Fang, X., et al. (2019). Increase in cfc-11 emissions from eastern China based on atmospheric observations. *Nature*, *569*(7757), 546–550. <https://doi.org/10.1038/s41586-019-1193-4>
- Saboya, E., Manning, A. J., Levy, P., Stanley, K. M., Pitt, J., Young, D., et al. (2024). U.K. N2O top-down emissions: Results from InTEM and RHIME 2013-2022. [Dataset]. Retrieved from <https://doi.org/10.5281/zenodo.10552071>. Zenodo
- Say, D., Manning, A. J., Western, L. M., Young, D., Wisner, A., Rigby, M., et al. (2021). Global trends and european emissions of tetrafluoromethane (cf4), hexafluoroethane (c2f6) and octafluoropropane (c3f8). *Atmospheric Chemistry and Physics*, *21*(3), 2149–2164. <https://doi.org/10.5194/acp-21-2149-2021>
- Sgouridis, F., & Ullah, S. (2017). Soil greenhouse gas fluxes, environmental controls, and the partitioning of n2o sources in UK natural and seminatural land use types. *Journal of Geophysical Research: Biogeosciences*, *122*(10), 2617–2633. <https://doi.org/10.1002/2017JG003783>
- Skiba, U., Jones, S. K., Dragosits, U., Drewer, J., Fowler, D., Rees, R. M., et al. (2012). UK emissions of the greenhouse gas nitrous oxide. *Philosophical Transactions of the Royal Society B: Biological Sciences*, *367*(1593), 1175–1185. Retrieved from <https://doi.org/10.1098/rstb.2011.0356>
- Stanley, K. M., Grant, A., O'Doherty, S., Young, D., Manning, A. J., Stavert, A. R., et al. (2018). Greenhouse gas measurements from a UK network of tall towers: Technical description and first results. *Atmospheric Measurement Techniques*, *11*(3), 1437–1458. <https://doi.org/10.5194/amt-11-1437-2018>
- Stavert, A. R., O'Doherty, S., Stanley, K., Young, D., Manning, A. J., Lunt, M. F., et al. (2019). UK greenhouse gas measurements at two new tall towers for aiding emissions verification. *Atmospheric Measurement Techniques*, *12*(8), 4495–4518. <https://doi.org/10.5194/amt-12-4495-2019>
- Stell, A. C., Bertolacci, M., Zammit-Mangion, A., Rigby, M., Fraser, P. J., Harth, C. M., et al. (2022). Modelling the growth of atmospheric nitrous oxide using a global hierarchical inversion. *Atmospheric Chemistry and Physics*, *22*(19), 12945–12960. <https://doi.org/10.5194/acp-22-12945-2022>
- Thompson, R. L., Chevallier, F., Crotwell, A. M., Dutton, G., Langenfelds, R. L., Prinn, R. G., et al. (2014). Nitrous oxide emissions 1999 to 2009 from a global atmospheric inversion. *Atmospheric Chemistry and Physics*, *14*(4), 1801–1817. <https://doi.org/10.5194/acp-14-1801-2014>
- Thompson, R. L., Gerbig, C., & Rödenbeck, C. (2011). A bayesian inversion estimate of n2o emissions for western and central europe and the assessment of aggregation errors. *Atmospheric Chemistry and Physics*, *11*(7), 3443–3458. <https://doi.org/10.5194/acp-11-3443-2011>
- Thompson, R. L., Lassaletta, L., Patra, P. K., Wilson, C., Wells, K. C., Gressent, A., et al. (2019). Acceleration of global n2o emissions seen from two decades of atmospheric inversion. *Nature Climate Change*, *9*(12), 993–998. <https://doi.org/10.1038/s41558-019-0613-7>
- Tian, H., Xu, R., Canadell, J. G., Thompson, R. L., Winiwarter, W., Suntharalingam, P., et al. (2020). A comprehensive quantification of global nitrous oxide sources and sinks. *Nature*, *586*(7828), 248–256. <https://doi.org/10.1038/s41586-020-2780-0>
- UK Committee on Climate Change. (2015). The fifth carbon budget: The next step towards a low-carbon economy. *Technical Reports Series*. Retrieved from <https://www.theccc.org.uk/publication/the-fifth-carbon-budget-the-next-step-towards-a-low-carbon-economy/>
- UK Department for Business Energy and Industrial Strategy. (2022). Updated energy and emissions projections 2021 to 2040 (Tech. Rep.). Retrieved from <https://www.gov.uk/government/publications/energy-and-emissions-projections-2021-to-2040>
- UK Department for Energy Security and Net Zero. (2022). Energy and emissions projections: 2021 to 2040 (tech. Rep.). Retrieved from <https://www.gov.uk/government/publications/energy-and-emissions-projections-2021-to-2040>
- UK Government. (2008). Climate change act 2008: Elizabeth ii. chapter 27.
- Wagner-Riddle, C., Congreves, K. A., Abalos, D., Berg, A. A., Brown, S. E., Ambadan, J. T., et al. (2017). Globally important nitrous oxide emissions from croplands induced by freeze-thaw cycles. *Nature Geoscience*, *10*(4), 279–283. <https://doi.org/10.1038/ngeo2907>
- Wells, K. C., Millet, D. B., Bousserez, N., Henze, D. K., Griffis, T. J., Chaliyakunnel, S., et al. (2018). Top-down constraints on global n2o emissions at optimal resolution: Application of a new dimension reduction technique. *Atmospheric Chemistry and Physics*, *18*(2), 735–756. <https://doi.org/10.5194/acp-18-735-2018>
- Western, L. M., Redington, A. L., Manning, A. J., Trudinger, C. M., Hu, L., Henne, S., et al. (2022). A renewed rise in global hfc-141b emissions between 2017-2021. *Atmospheric Chemistry and Physics*, *22*(14), 9601–9616. <https://doi.org/10.5194/acp-22-9601-2022>
- Xiang, B., Miller, S. M., Kort, E. A., Santoni, G. W., Daube, B. C., Commancin, R., et al. (2013). Nitrous oxide (n2o) emissions from California based on 2010 calnex airborne measurements. *Journal of Geophysical Research: Atmospheres*, *118*(7), 2809–2820. <https://doi.org/10.1002/jgrd.50189>